

# Intensity Variation of Large Solar Energetic Particle Events Associated with Coronal Mass Ejections

N. Gopalswamy,<sup>1</sup> S. Yashiro,<sup>1,2</sup> S. Krucker,<sup>3</sup> G. Stenborg,<sup>1,2</sup> and

R. A. Howard<sup>4</sup>

---

N. Gopalswamy, S. Yashiro and G. Stenborg, NASA Goddard Space Flight Center, Greenbelt, MD 20771, USA. (gopals@fugee.gsfc.nasa.gov; yashiro@cdaw.gsfc.nasa.gov; stenborg@kreutz.nascom.nasa.gov)

S. Krucker, Space Sciences Laboratory, University of California at Berkeley, Berkeley, CA 94720, USA. (krucker@ssl.berkeley.edu)

R. A. Howard Solar Physics Branch, Space Sciences Division, Naval Research Laboratory, Washington, D. C., 20375, USA. (russ.howard@nrl.navy.mil)

<sup>1</sup>NASA Goddard Space Flight Center,  
Greenbelt, Maryland, USA.

<sup>2</sup>The Catholic University of America,  
Washington, D. C., USA.

<sup>3</sup>University of California at Berkeley,  
Berkeley, California, USA.

<sup>4</sup>Naval Research Laboratory, Washington,  
D. C., USA.

**Abstract.**

We studied the coronal mass ejections (CMEs) and flares associated with large solar energetic particle (SEP) events of solar cycle 23 (1996-2002) in order to determine what property of the solar eruptions might order the SEP intensity. The SEP events were divided into three groups: (i) events in which the primary CME was preceded by one or more wide CMEs from the same solar source, (ii) events with no such preceding CMEs, and (iii) events in which the primary CME might have interacted with a streamer, or with a nearby halo CME. The SEP intensities are distinct for groups (i) and (ii) although the CME properties were nearly identical. Group (iii) was similar to group (i). The primary findings of this study are (1) Higher SEP intensity results whenever a CME is preceded by another wide CME from the same source region. (2) The average flare size was also larger for high intensity SEP events. (3) The intensity of SEP events with preceding CMEs showed a tighter correlation with CME speed. The extent of scatter in the CME speed vs. SEP intensity plots was reduced when various subgroups were considered separately. (4) The intensity of energetic electrons were better correlated with flare size than with CME speed. (5) The SEP intensity showed poor correlation with the flare size, except for group (iii) events. Since only a third of the events did not have preceding CMEs, we conclude that the majority of SEP producing CMEs propagate through the near-Sun interplanetary medium severely disturbed and distorted by the preceding CMEs. Furthermore, the preceding CMEs are faster and wider on the average, so they may provide seed particles for CME-driven shocks that follow. Therefore, we conclude that

the differing intensities of SEP events in the two groups may not have resulted due to the inherent properties of the CMEs. The presence of preced-

## 1. Introduction

Although the close relationship between interplanetary (IP) shocks and the observed time profiles of solar energetic particle (SEP) events was recognized long ago [*Obayashi*, 1962], the connection between shocks and coronal mass ejections (CMEs) got the attention soon after the discovery of white light CMEs [*Stewart et al.*, 1974]. The importance of CME occurrence for the production of SEPs was first demonstrated by *Kahler et al.* [1978], leading to the suggestion that SEPs may be accelerated by the shock ahead of CMEs. It is currently thought that the large, gradual, and long-lived SEP events are due to CME-driven shocks [*Reames*, 1999]. However, there is still no widely accepted theory that explains all the observed properties of SEPs. For example, the CME speed and SEP intensity are reasonably correlated, yet the scatter is very large: for a given CME speed, the SEP intensity can vary over four orders of magnitude, with no satisfactory explanation at sight [*Kahler* 2001; *Gopalswamy et al.*, 2003a]. The presence pre-existing of SEPs in the ambient medium and variations of energy spectra among SEP events are thought to be significant factors that can account for 1 to 2 orders of magnitude variation in SEP intensities [*Kahler*, 2001]. The ambient SEPs are supposed to form a seed population, which are further accelerated by the CME-driven shocks. The seed particles may originate from impulsive flares [*Mason et al.*, 1999] or from preceding CMEs [*Gopalswamy et al.*, 2002a]. In addition to the presence of seed particles, the physical conditions in the ambient medium may also modify the characteristics of shocks and hence affect the intensity of SEPs. In a preliminary study, *Gopalswamy et al.* [2003a] found that SEP events of cycle 23 (1997-2001) preceded by wide CMEs from the same source region within a day were more likely to have higher intensities than those without such preceding CMEs. However, they

did not evaluate how the correlation between SEP intensity and CME speed was affected by the presence of preceding CMEs. In this paper, we study this correlation for all large SEP events of solar cycle 23 (from 1996 to the end of 2002), identify their solar sources, and study the properties of the associated CMEs. For the subgroup with preceding CMEs, we compare the properties of the SEP-related CMEs with those of preceding CMEs. Since CME-driven shocks are thought to accelerate both electrons (inferred from type II radio bursts) and ions, we extend the study to energetic electrons detected in situ to see if the electron flux is affected by the presence of preceding CMEs. Finally, we examine the correlation between energetic proton and electron intensities with the flare size.

FIGURE

## 2. Data Selection

### 2.1. SEP Events

We started with the set of all large proton events (intensity  $\geq 10$  pfu, with  $1 \text{ pfu} = 1 \text{ proton cm}^{-2} \text{ s}^{-1} \text{ sr}^{-1}$ ) in the  $> 10$  MeV channel of the GOES instrument from 1997 to 2002. GOES data are available on line from NOAA Space Environment Center (<http://sec.noaa.gov>). We excluded six events that occurred during the period of temporary disability (June to October, 1998 and January to February, 1999) of the Solar and Heliospheric Observatory (SOHO) mission because the CME data in this study were obtained by SOHO's Large Angle and Spectrometric Coronagraph (LASCO, *Brueckner et al.*, 1995). The C2 and C3 telescopes of LASCO obtain images of the corona from  $\sim 2$  to  $32 R_s$  field of view (FOV) from which the characteristics of CMEs are measured. For 8 events the higher intensity may be due to shock spike or interplanetary (IP) modulation of previous events, so they are not included in the analysis. Table 1 lists the remaining

<b>Table 1</b>
----------------

60 intervals with SEP intensity exceeding 10 pfu. The event number (No.), SEP date, and onset time at GOES are given in columns 1-3, respectively. For each of these SEP events, we were able to identify a unique CME (which we call the primary CME). We have compiled the properties of the primary CMEs such as the time (T2) of first appearance in the LASCO/C2 FOV, speed (V2 km s<sup>-1</sup>), width (W2 deg), and mass (M in 10<sup>15</sup> g) in columns 4-7. The masses of the primary CMEs were determined using the standard technique of estimating the CME volume and the number of electrons contained in the CME [Vourlidas *et al.*, 2002]. The solar source location of the CMEs was identified using a number of data sources (images, movies and lists) such as (i) the online Solar Geophysical Data, movies from SOHO's Extreme-ultraviolet imaging telescope [EIT, *Delaboudiniere et al.*, 1995], movies from the soft X-ray telescope (SXT) on board the Yohkoh spacecraft (until December 2001), microwave movies from the ground based Nobeyama radioheliograph [Nakajima *et al.*, 1994], and TRACE movies. We also used data collected during the Living With a Star (LWS) Coordinated Data Analysis Workshop (LWS/CDAW) held in July 2002 (<http://cdaw.gsfc.nasa.gov/LWS/>). The sources identified in this way are listed in Table 1 as a heliographic location (latitude and longitude in column 8). When the solar source is behind the limb, the position angle can be identified from EIT movies and the solar source is indicated to be beyond the appropriate limb. For example, >NW90 means that the source is behind the northwestern limb of the Sun. The corresponding NOAA active region (AR) number, if available, is given in column 9. From the Solar Geophysical Data, we identified the flare size (X-ray/optical importance in column 10) and onset time of GOES soft X-ray flares (column 11). In columns 12 and 13, we have indicated the onset times of the associated metric and decameter-hectometric (DH) type

II radio bursts; N denotes the lack of a radio burst. In order to compare the association of the SEP events with the corresponding energetic electron events, we use the in-situ electron measurements taken by the Three-dimensional Plasma and Energetic Particle (3DP) instrument [Lin *et al.* 1995] on the Wind spacecraft. Solid state detectors covering the range between 30 and 500 keV provide the best signal to noise ratio. This energy range is normally grouped into 7 logarithmically binned channels. For each energy channel the intensity of the electron event (in units of electron flux units or efu; 1 efu = 1 electron  $\text{cm}^{-2} \text{s}^{-1} \text{sr}^{-1} \text{eV}^{-1}$ ) was determined as the maximal flux observed during the event. Since impulsive electron events very often show velocity dispersion - higher energy electrons arrive before the lower energy ones - the peak fluxes at different energies are generally taken at different times. In this paper, we consider data from only one channel (108 keV), because at this energy the electrons have roughly the same speed as the  $> 10$  MeV protons. The proton intensity ( $I_p$ ) and 108 keV electron flux ( $I_e$ ) are listed in Table 1.

## 2.2. Subgroups of SEP Events

In order to assess the influence of the medium, we examined the conditions prevailing the corona into which the primary CMEs were launched. A certain volume of the corona is disturbed if there was a recent CME in that part of the corona. In order to quantify this we searched for other CMEs from the same source region as the primary CME that satisfy the following two criteria: (i) the preceding CMEs should have been launched within 24 hours ahead of the onset time of the primary CMEs, and (ii) the preceding CMEs must be wider than average CMEs. Since the average width of non-halo CMEs is  $\sim 47^\circ$ , CMEs having a width  $\geq 60^\circ$  are deemed wide. If there were more than one

preceding CME satisfying the above criteria, we choose the CME closest in time to the primary CME. Since it takes less than one day to more than 4 days for CMES to reach Earth [*Gopalswamy et al.*, 2000a; 2001], choosing 1 day precedence makes sure that the aftermath of the preceding CMES is not relaxed back to the pre-eruption conditions when the primary CME starts out. (Figure 1) shows an SEP event with a preceding CME. The preceding (CME1) and primary (CME2) CMES originated from the same solar source (AR 9628) located close to the southwest limb as can be seen in the EIT difference images. In the LASCO/C3 image at 06:18 UT, both CME1 and CME2 can be seen. The proton intensity at three energy channels is also shown. The peak intensity in the  $>10$  MeV channel is 2360 pfu. In the CME height-time plots, the onset times of the two CMES and their difference ( $\Delta T$ ) are marked. The trajectories intersect at a height of  $\sim 18 R_s$ . When the primary CME lifts off, the preceding CME is already at a height of  $\sim 12 R_s$ . We denote this initial separation between the primary and preceding CMES as  $\Delta R$ . The GOES light curves show the flare associated with the primary CME in the 1.0-8.0 Å and 0.5-4.0 Å channels, with the heliographic location (S20W84) marked. The flare associated with the preceding CME was not listed in the Solar Geophysical Data, but the eruption was clearly seen in SOHO/EIT images. There were 23 such SEP events in which the primary CMES were ejected into the aftermath of preceding CMES, as listed in Table 2. The onset time ( $T_1$ ) of the preceding CME, its speed ( $V_1$ ,  $\text{km s}^{-1}$ ), and width ( $W_1$ , deg) are given in columns 5-7. The heliographic locations (column 8) and the active region numbers (column 9) are also included. The preceding time interval ( $\Delta T$  in hours), the initial spatial separation ( $\Delta R$  in  $R_s$ ) and the approaching speed ( $\Delta V = V_2 - V_1$   $\text{km s}^{-1}$ ) are given in columns 10-12. The intensity ( $I_p$  in pfu) of the proton event associated with

**Figure 1**

**Table 2**

the primary CME is given in column 13. The last column (14) contains information on the kind of energetic activity is associated with the preceding CMEs: complex type III bursts (cxIII), simple type III bursts (III or DHIII), metric type II bursts (MII), DH type II bursts (DHII), and minor ( $(I_p < 10 \text{ pfu})$  SEP events (minor). It must be pointed out that  $\Delta T$  was obtained by extrapolating the linear fit to the height-time measurements in the sky plane to  $1 R_s$ , and taking the difference between the two onset times.  $\Delta T$  is generally not too different from  $T_2 - T_1$ .  $\Delta T$  and  $\Delta V$  indicate the extent of interaction between the primary and preceding CMEs. For example a small  $\Delta T$  and a large  $\Delta V$  correspond to CMEs that interact very close to the Sun. This group of 23 SEP events will be henceforth referred to as ‘P’ events to note that the primary CMEs were preceded by at least one wide CME.

For a group of 20 events, the opposite situation applies: we cannot find a preceding wide CME for any of these from the same source region as the primary CME. We call these as ‘NP’ events to note that there were ‘No Preceding’ CMEs. Fig. 2 shows an example of the NP events (event #17 in Table 1). Three snapshots of the LASCO images are shown superposed on EIT difference images with the source region (S17W09) pointed by arrows. The CME originated from a quiescent filament region. The filament eruption resulted in a prominent EUV and X-ray post-eruption arcade with an M-class X-ray flare. The event had a proton intensity of 320 pfu. While there were two large CMEs from other parts of the Sun following the primary event, there was no preceding eruption from the filament region in question.

**Fig. 2**

The remaining 17 events could not be included in either group due to various reasons described below:

(1) One event was completely back-sided (event #33, *Gopalswamy, 2002*) so it is difficult to say whether there was a preceding CME or not. Therefore, this event was dropped from the statistical analysis.

(2) For another event (#32, 2001 August 09) it was not possible to unambiguously identify the primary CME responsible for the SEP event. There was a candidate CME, a partial halo associated with a filament eruption near the central meridian, as indicated by the post-eruption arcade in Fig. 3. The CME was gradually accelerating with an average speed of only  $479 \text{ km s}^{-1}$ . The speed was still under  $600 \text{ km s}^{-1}$  by the time the CME left the LASCO field of view at 19:32 UT. The CME seems to have lifted off too early (at 10:30 UT,  $\sim 8.5 \text{ h}$  before the SEP onset). The EIT images showed another clear eruption later in the day from close to the disk center (AR 9570 at S17E19) at 18:22, but no white light CME was observed. Soft X-ray images from Yohkoh/SXT show that the sources of these two eruptions were separated by a large coronal hole extending from the south polar region into the northern hemisphere (see Fig. 3). This coronal hole is likely to deflect the nearby CMEs and prevented easy detection of a possible CME from AR 9570. This coronal hole might have also been responsible for the confinement of the 10:30 UT CME to the western hemisphere. Since it is difficult to decide between the two eruptions, we drop this event from further analysis.

**Fig. 3**

**Fig. 3**

(3) For 6 events (#03, #19, #20, #48, #49, and #52), there were major preceding eruptions from the source regions indicative CMEs, but the primary CMEs followed so closely that they would have overtaken any preceding CMEs within the occulting disk of LASCO coronagraph. The preceding eruptions were clearly observed in the inner coronal images such as from SOHO/EIT, Yohkoh/SXT and the Nobeyama Radioheliograph

[*Gopalswamy, 2004a*]. Figure 4 shows an example from 2002 March 15 (event #48). Two eruptions can be seen in the EIT difference images at 22:00 and 22:36 UT corresponding to the two peaks in GOES soft X-ray plot. The first eruption produces a dimming to the northwest of AR 9866, while the second one is more extensive with a dimming to the South of the same AR. The LASCO image at 23:06 shows a single CME with a complex front. Such CMEs should belong to group P, but we cannot use them in the statistical analysis since the preceding CMEs could not be measured. The onset time difference between the associated flares can be used, but there is no information on  $\Delta V$ .

**Figure 4**

(4) For 7 other events (#22, #34, #39, #43, #45, #46, and #57), the primary CME interacted with a nearby streamer. Since streamers are the pre-eruption stages of CMEs, they may be considered as preceding CMEs of “zero speed”. Figure 5 shows an example of the streamer interaction events. This is event # 43 in Table 1 that occurred on 2001 December 26 from AR 9742 (N08W54). There was a streamer located above the west limb at PA  $\sim 300^\circ$  as marked in the 04:54 UT LASCO image. The streamer had appeared above the west limb for the first time on 2001 December 18. There were some slow CME events apparently originating from the outer layers of the streamer without affecting its overall structure. In the 05:30 UT image on 2002 March 15, the CME can be seen above the west limb with the solar source visible in EIT image as a brightness enhancement. In the image at 06:54 UT, the streamer is completely blown off. The primary CME on 2001 December 26 resulted in an SEP event of 779 pfu, certainly an order of magnitude above the threshold we set for high intensity events. The CME was fast ( $1446 \text{ km s}^{-1}$ ) and wide (width  $\geq 212^\circ$ ). In a sense these streamer interactions are similar to the close-to-source interactions because in either case we cannot derive the properties of preceding CMEs.

**Figure 5**

(5) Event # 41 should belong to the NP group since there was no preceding wide CME. However, during its rise phase next event (# 42) from a nearby region started during its rise phase, so we could not determine the proton flux. Therefore, this event will be excluded from analysis. Event #42 did not have a preceding CME from the same region, but the interaction of its primary CME with that of event #41 has been documented [Gopalswamy *et al.*, 2003a]. Both were halo CMES originating from neighboring active regions. For this reason, we treat this event as a special case (halo-halo interaction) in the analysis.

To summarize, there are 57 well-observed large SEP events that can be divided into three groups: (i) 23 P events in which the the primary CMES were preceded by other wide CMES, (ii) 20 NP events events in which the the primary CMES were not preceded by other wide CMES, and (iii) 14 O events, in which “Other” types of interaction (below the occulting disk interactions, streamer interactions and halo-halo interaction) occurred and hence these cannot be included in the NP group. We primarily consider the P and NP groups for studying the influence of CME interaction on SEP intensity. The O events will be used for consistency check.

### 3. Analysis and Results

We are interested in the properties of the P and NP events and seek their differences in terms of (i) the intensity of the energetic proton and electron events, (ii) the speed, width, mass, source longitude, and kinetic energy of the primary CMES, and (iii) the associated flare size, and (iv) the correlation between the proton intensity and CME speed, and (v) the correlation between energetic electron intensity and CME speed.

### 3.1. Particle Intensities

Figure 6 shows the distributions of proton and electron intensities of the 57 events in comparison with those of the P and NP events. Energetic electrons were detected only in 45 of the 57 events. For both protons and electrons, the intensity of P events extends to much larger values compared to that of NP events. For example, the median intensity of protons is 210 pfu for the P events, compared to just 29 pfu for the NP events. The results did not change when we considered only the frontside events (the darker histograms in Fig. 6). The median value for the entire set of 57 events is 54 pfu, which seems to be an intensity value that demarcates the P and NP events. The intensity difference can also be clearly seen for the electron events. The ratios of various median values are shown in Table 3. The median value of the NP events,  $I(\text{NP})$ , is half the median value  $I(\text{ALL})$  for the 57 events taken together. This result applies for both electrons and protons. On the other hand, the median intensity of the P events,  $I(\text{P})$ , is four times  $I(\text{ALL})$  for protons and twice  $I(\text{ALL})$  for electrons. Furthermore,  $I(\text{P})$  is  $\sim 7$  times and  $\sim 4$  times  $I(\text{NP})$  for protons and electrons, respectively.

On the basis of the distributions shown in Fig. 6, SEP events with proton intensity ( $I_p$ )  $\geq 50$  pfu will be referred to as high-intensity events; those with  $I_p < 50$  pfu, will be referred to as low-intensity events. From Table 1, we see that the majority (18/23 = 78%) of the P events are of high intensity. On the other hand, only 5 of the 20 (25%) NP events had high intensity. Furthermore, only two of the 20 NP events (10%) had  $I_p > 100$  pfu, while 13 of the 18 (72%) P events had  $I_p > 100$  pfu. Thus CMEs that propagate into the aftermath of preceding CMEs are  $>3$  times more likely to be associated with high-intensity SEP events (see also Tables 3 and 4).

**Figure 6**

**Table 3**

**Tables 3 a**

### 3.2. Properties of Primary CMES

Figure 7

Are there other differences between the CMES of P and NP events? Figure 7 compares the speed, width, and the source longitudes of the two groups with those of all the 57 events listed in Table 1. First of all, we confirm that the average speed ( $1468 \text{ km s}^{-1}$ ) of SEP-producing CMES is about three times as large as the average speed of the general population [Gopalswamy *et al.*, 2002a]. The average CME speeds of P ( $1492 \text{ km s}^{-1}$ ) and NP ( $1499 \text{ km s}^{-1}$ ) events are nearly identical. Most of the CMES in the two groups were halo CMES ( $18/23 = 72\%$  in group P and  $15/20 = 75\%$  in group NP). There is no CME in either group with width less than  $\sim 120^\circ$ . Furthermore, the two groups have similar speeds and widths as the entire set of 57 SEP-associated CMES. As for the longitude distribution, we see that there is a general tendency for the SEP events to occur in the western hemisphere. The tendency is more pronounced for the P events than for the NP events. About half of the NP events originated from beyond the limb, while only three of the group P events were behind the limb. One might argue that behind-the-limb sources mean poor connectivity for detection at Earth and hence the group NP events may be of low intensity. However, as we showed in Figure 6, even if we consider just the front-side events, the intensity difference between P and NP events persisted. In other words, when the frontside events alone are considered, the primary distinction between the two groups is indeed the presence of preceding CMES. The average speed of the frontside NP CMES is  $1378 \text{ km s}^{-1}$  compared to the  $1618 \text{ km s}^{-1}$  for the behind-the-limb NP events. This slight difference ( $\sim 15\%$ ) is not significant because the limb events have little projection effects and hence tend to show a higher speed compared to the disk events [Gopalswamy *et al.*, 2000b].

### 3.3. Mass and Kinetic Energy of CMES

The CME mass is estimated by determining its volume and the number of electrons contained in it, assuming the CME to be a fully-ionized hydrogen plasma with 10% helium. The average mass of LASCO CMES is  $\sim 1.6 \times 10^{15}$  g, slightly lower than those of pre-SOHO CMES [see, e.g. *Vourlidas et al.*, 2002]. For the primary CMES, the average and median masses are much higher than this value (see Fig. 8a-c). For the 50 events for which we were able to make a mass estimate, the masses were in the range  $\sim 5 \times 10^{15}$  g to  $\sim 3 \times 10^{16}$  g, with a median value of  $\sim 9 \times 10^{15}$  g. The primary CMES of the P and NP events had nearly the same median mass, suggesting that the CME mass is not a distinguishing characteristic between the two groups. Since there is little difference in the speed and mass between the two groups, we do not expect the kinetic energies to be different either. The median kinetic energy for the 50 SEP events with mass measurements was  $8.5 \times 10^{31}$  erg. For the P and NP groups, the median values were  $7.1 \times 10^{31}$  erg and  $1.0 \times 10^{32}$  erg, respectively. However, the kinetic energy of the SEP-related CMES is an order of magnitude larger than the average and median kinetic energies of the general population of CMES [*Vourlidas et al.*, 2002; *Gopalswamy*, 2004b].

Fig. 8a-c

### 3.4. Flare size

We now compare the sizes of the flares associated with the P and NP events. We use the peak soft X-ray flux (in units of  $\text{W m}^{-2}$ ) during the flare in the GOES 1-8 Å channel as a measure of the flare size. To be observed, the flares have to occur on the front side with no occultation by the limb. There were 45 events in all for which the soft X-ray intensity of the flare is available (see Table 1). The distribution of flare sizes is shown in Fig. 8(g-i). The flare sizes varied over three orders of magnitude with a median value of

$7.1 \times 10^{-5} \text{ W m}^{-2}$  for the 45 events. However, when the P and NP events are considered separately, there is a clear difference: The NP events have an average peak X-ray flux ( $3.9 \times 10^{-5} \text{ W m}^{-2}$ ), which is  $\sim 5$  times smaller than that ( $2.1 \times 10^{-4} \text{ W m}^{-2}$ ) of the P events. In addition to the presence of preceding CMES, the flare size seems to be another parameter that distinguishes the two groups of events.

### 3.5. Type II Radio Bursts

Radio bursts of type II are indicative of MHD shocks in the corona (inferred from metric type II bursts) and IP medium (inferred from DH and longer wavelength type II bursts). When we compare the onset times of metric and DH type II bursts with those of CMES in Table 1, it is clear that they are closely related phenomena. In an earlier report, Gopalswamy (2003) found that 70-80% of the large SEP events were associated with metric type II bursts while 100% of them were associated with DH type II bursts. With the expanded data set of the present study (see Table 1), the earlier results are confirmed: 45 of the 57 SEP events (or 79%) were associated with metric type II bursts while all the 60 (or 100%) of them were associated with DH type II bursts. This close relationship between type II bursts and SEP events has been taken to indicate that the same CME-driven shock accelerates electrons responsible for the type II bursts and SEPs detected in situ. It is interesting to note that there is no difference among P, NP and O events in terms of their association with DH type II bursts. The deficit of metric type II bursts is roughly the same for P, NP and O events: 17%, 20%, and 29%, respectively. We conclude that there is no major difference between P and NP events in terms of their association with type II radio bursts.

#### 4. Properties of Preceding CMES

The speed, width, and longitude distributions of the preceding CMES (see Table 2) are compared with those of the primary CMES in Fig. 9. The average speed ( $715 \text{ km s}^{-1}$ ) of the preceding CMES is much smaller than that ( $1492 \text{ km s}^{-1}$ ) of the primary CMES. However, the average speed of the preceding CMES is significantly larger than that of the general population of LASCO CMES ( $\sim 488 \text{ km s}^{-1}$ , see *Gopalswamy et al.*, 2003b; *Yashiro et al.*, 2004; *Gopalswamy*, 2004b). This is expected on the basis of our selection criterion that the preceding CMES must be wide ( $\geq 60^\circ$ ) because width and speed are correlated [see, e.g., *Yashiro et al.*, 2004]. What is the implication of the above-average speed of preceding CMES? According to *Gopalswamy et al.* [2001a], the fast mode speed outside the core of active regions has a broad peak at a heliocentric distance of  $\sim 3 R_s$  with a peak value of  $550 \text{ km s}^{-1}$ . The peak value depends on the actual density and magnetic field values. At coronal levels where metric type II bursts originate, the fast mode speed could be substantially lower than the peak value, so CMES can easily drive shocks, provided their starting height is low enough. The preceding CMES, with an average speed well above the peak Alfvén speed, are likely to drive shocks near the Sun and hence accelerate some particles, which may serve as seed particles for the shock of the primary CME. In order to show that the preceding CMES may drive shocks, we examined the radio bursts associated with the preceding CMES. Table 2, we have indicated the type of radio phenomena associated with the preceding CMES (mII - metric type II; DH II - type II bursts in the decameter-hectometric (DH) wavelength regime; cxIII - complex type III bursts generally associated with large CMES). The majority (13/23 or  $\sim 57\%$ ) of the preceding CMES had either metric or DH type II bursts, indicative of shocks near

Fig. 9

the Sun. Four of the 13 CMEs had also minor SEP events ( $I_p \leq 1$  pfu), because these 4 CMEs had an average speed of  $915 \text{ km s}^{-1}$ . Figure 9 also shows that three-quarters of the preceding CMEs had widths exceeding  $90^\circ$ . The lower cutoff at  $60^\circ$  is due to the selection criterion used. Thus the above-average width of the preceding CMEs is also consistent with their ability to drive shocks because DH type II bursts are invariably associated with fast and wide CMEs [Gopalswamy *et al.*, 2001c].

#### 4.1. Primary and Preceding CMEs: Spatial and Temporal Relationship

Figure 10 shows the distributions of (a) temporal separation ( $\Delta T$ ), (b) the approaching speed ( $\Delta V$ ), and (c) initial spatial separation ( $\Delta R$ ) between primary and preceding CMEs.  $\Delta T$  ranges between  $<1$  h and 24 h (the upper limit is due to our selection criterion). Interestingly, the average preceding time was only  $\sim 11$  h. The average approaching speed is relatively high ( $777 \text{ km s}^{-1}$ ) suggesting that the primary CMEs would catch up with the preceding CMEs in the near-Sun IP medium. Fig. 10c shows that at the lift-off time of the primary CMEs, the preceding CMEs are typically at a heliocentric distance of  $\sim 35 R_s$ , close to the outer edge of the LASCO FOV. At the onset time of the primary CMEs, the preceding CMEs were located anywhere from  $\Delta R < 2$  to  $\sim 90 R_s$ , but generally closer to the Sun, than to Earth. The mean and median values of  $\Delta R$  were 35 and 37  $R_s$ , respectively. Finally, Fig. 10d shows the heliocentric distance at which the primary CME would have caught up with the preceding CMEs. This distance was obtained by simply extrapolating the height-time plots for primary and preceding CMEs up to the point where the two trajectories would intersect. While this is a reasonable estimate for the limb events, it may not be so for disk events and for those events which show gradual acceleration. Nevertheless, it provides an estimate of the distance at which

**Figure 10**

the CMES would have completed interaction. The mean value of this “interaction height” is  $69 R_s$ . *Gopalswamy et al.* [2002a] obtained similar results with less restrictive criteria on the source region and width of the preceding CMES: the preceding CMES were required to have a position-angle overlap with the primary CMES. They obtained a height of intersection to be  $\sim 21 R_s$ , and the temporal separation as  $\sim 7$  h. They also obtained the average width of the preceding CMES to be  $\sim 50^\circ$ .

## 5. Particle Intensity - CME speed relationship

The good correlation between SEP intensity and CME speed has been considered as a strong evidence supporting the paradigm that SEPs are accelerated by CME-driven shocks [see e.g., *Kahler* 2001, and references therein]. The SEP intensity is generally better correlated with CME speed than with the flare size [*Gopalswamy et al.*, 2003a]. However, the scatter is very large, to the extent that for a given CME speed the SEP intensity could vary over 3-4 orders of magnitude. *Kahler* [2001] suggested that the presence of SEPs in the IP medium might be able to account for one order of magnitude in the scatter. If we accept the paradigm that all large SEP events originate from CME-driven shocks, then the background SEPs in the IP medium might be due to preceding CMES. In other words, our P events are somewhat similar to *Kahler* [2001] events that occur when background SEPs are present. The difference, of course, is that we are considering preceding CMES based on white light observations, while *Kahler* [2001] considers background SEPs detected in situ.

In order to see the effect of preceding CMES, we have made scatter-plots between the SEP intensity and CME speed for the two groups in Fig. 11. We have made two sets of plots, one with all the events and the other with only frontside events (—longitudes—

**Fig. 11**

$\leq 90^\circ$ ). Clearly, the correlation coefficients ( $r$ ) for the P (0.43) and NP (0.58) events are similar to the values obtained before [Kahler, 2001; Gopalswamy et al., 2003a]. When we exclude events from behind the limb, the correlation improves dramatically for the P events ( $r$  increases from 0.43 to 0.70) while it slightly decreases for the NP events (from 0.58 to 0.46). The two outliers that caused poorer correlation for the P events are behind-the-limb events. The scattering is also reduced compared to the total plot. We see that the P and NP events occupy distinct regions in the CME speed- $I_p$  plot. When we consider the P and NP events together, the correlation coefficients are 0.36 and 0.52, respectively for all and frontside events, respectively.

The effect of preceding CMEs on the correlation between SEP intensity and CME speed is shown in Fig. 12. The largest extent of scatter is seen when the two groups are combined. When front-sided events alone are considered, the extent of scatter did not decrease significantly for the combined data set. When considered separately, the extent of scatter is reduced significantly for the P and NP events. When front-sided events alone are considered, there is further reduction of scatter for the P events with little change for the NP events.

Fig. 12

### 5.1. Electron Intensity - CME speed Relationship

The scatter plots between the electron flux and CME speed are shown in Fig. 13. The electron flux is hardly correlated with CME speed for both P and NP populations. When we exclude the behind-the-limb events, the correlation improves slightly for the P events, while there is hardly any change for the NP events. From the electron events alone, it is difficult to see the effect of preceding CMEs, but is consistent with the relationship

Fig. 13

indicated by proton events. However, the scatter plot clearly shows the different regions occupied by the P and NP electron events.

## 5.2. Other Possible Interactions

In the above analysis, we had excluded the O events (streamer interactions, possible interaction below the occulting disk, and halo-halo interaction) because there is little information on the preceding CMEs that could be used for statistical investigation. In order to see how these interactions affect the particle intensity - CME speed correlation, we have made scatter plots for protons (Fig. 14) and electrons (Fig. 15) including the O events. The correlation coefficient for the O events ( $r=0.68$ ) is higher than that for the NP and P groups. Furthermore, when we exclude the single behind-the-limb event in the O group, the correlation coefficient for the non-limb events becomes  $r=0.74$ . The O events clearly merge with the P events and generally away from the NP events. Only 11 of the 14 O events were associated with energetic electrons and the correlation coefficient between electron intensity and CME speed ( $r = 0.78$ ) is similar to that of protons ( $r = 0.74$ ). We conclude that the O-type events clearly belong to the P group. When we combined the O and P groups, the correlation coefficients for protons were 0.45 (all) and 0.59 (front-sided). For electrons, the corresponding correlation coefficients were 0.29 and 0.45.

**Fig. 14**

**Fig. 15**

## 6. Particle Intensity and Flare size

The proton intensity is known to be weakly correlated with flare size measured as the peak 1-8 Å X-ray intensity [Gopalswamy *et al.*, 2003a]. We repeated the correlation analysis for the three subgroups (P, NP, and O) and the result is shown in Fig. 16.

**Fig. 16**

The proton intensity of NP events has no correlation with the flare size at all; for the P events, it has an extremely weak correlation ( $r=0.12$  for all events and  $0.22$  for front-sided events). The correlation coefficient for the O events is surprisingly high ( $r=0.71$  for all O events and  $0.78$  for front-sided events). The presence or absence of preceding CMES seems to make no difference for the correlation between the SEP intensity and flare size. This means the weak correlation found earlier between the SEP intensity and flare size [Gopalswamy *et al.*, 2003a] must be entirely due to the O events.

The correlation between electron intensity and flare size is shown in Fig. 17. First of all, we note that the electron flux of NP events is not correlated with the flare size. On the other hand the P events are highly correlated with the flare size ( $r=0.74$  for all events and  $0.86$  for front-sided events). The correlation is also very high ( $r=0.78$ ) for the O events, consistent with the previous conclusion that the O events behave very similar to the P events.

**Fig. 17**

Table 5 summarizes the various correlations discussed above. We see a clear tendency for the proton intensity of P and O events to have the best correlation with CME speed. On the other hand, electron intensity is best correlated with flare size again for the P and O events.

**Table 5**

## 7. What Causes High Intensity?

The primary result of this paper is that the high-intensity SEP events are predominantly associated with fast and wide CMES that are preceded by other wide CMES from the same source region within a day. This means, the primary CMES must be propagating through the preceding CMES or their aftermath, rather than through the normal corona/solar wind. During the first few hours of their life time, the shocks driven by the primary

CMEs are highly potent in accelerating particles [see, e. g., *Kahler*, 1994]. It is during this phase that the shocks driven by the primary CMEs propagate through a medium highly disturbed and distorted by the preceding CMEs. Although a detailed analysis of the physical mechanism by which the SEP intensity may be enhanced is beyond the scope of this paper, we would like to discuss a few possibilities. One can roughly divide the effects into three categories: (i) effects related to the modification of the primary shock, (ii) effects related to the deviation of the medium from normal solar wind (with Parker-spiral magnetic field), and (iii) presence of seed particles in the ambient medium.

It is easy to understand the modification of the primary shock because, shock strength (or Alfvénic Mach number) can change depending on the magnitude and distribution of the plasma density ( $n$ ) and magnetic field ( $B$ ) in the disturbed region. The change in the characteristic speed (Alfvén speed  $V_a$ , since the sound speed is relatively small) due to changes in  $n$  and  $B$  can be written as:  $dV_a/V_a = dB/B - (1/2) dn/n$ . Near the Sun, the density enhancement represented by the preceding CME may be important, which lowers  $V_a$  and makes the shock strong; stronger shocks would result in higher SEP intensity, which is known statistically and from theoretical considerations. This is consistent with the observed DH radio emission enhancement for a duration corresponding to the transit time of the primary shock through the density enhancement of a preceding CME observed by LASCO [*Gopalswamy et al.*, 2001b; 2002b].

A shock propagating through a normal solar wind may have most of its surface threaded by open field lines along which accelerated particles escape. When there is a preceding CME, the shock may be propagating through a mixture of closed and open field lines. Depending on the separation between the primary and preceding CMEs, some particles

escaping the primary shock may be returned for further acceleration by the closed field lines threading the primary shock. Implications of the presence of preceding CMEs as modifiers of the structure of the interplanetary magnetic field (on spatial scales of tenth of an AU) was considered by *Kallenrode* [2002] in a numerical model.

Presence of seed particles of both from CMEs [*Kahler*, 2001] and from preceding flares [*Mason et al.*, 1999] have been considered. These authors base their result on particles detected at 1 AU. We consider the presence of particles in the very early stages in a region directly overlying the primary shocks. It is worth noting that the aftermath of CMEs may contain dense core material which may be cold or hot [see e.g., *Ciaravella et al.*, 2003]. The cores may also contain nonthermal electrons, which produce moving type IV radio bursts known for more than four decades [see, e.g. *Stewart*, 1985]. It is likely that these plasmoids with nonthermal electrons may also carry low energy ions. When a primary shock encounters preceding CME with a nonthermal core, it can accelerate these particles further. Presence of type II bursts also indicates the presence of shock-accelerated electrons and the same shocks may accelerate low levels of ions.

The better correlation between electron flux and flare size for the P and O events needs further investigation. It is generally understood that the flare phenomenon observed in H-alpha and X-rays is due to the precipitation of energetic electrons into the chromosphere from the flare site in the corona. On the other hand the electrons detected in situ are the ones propagating away from the Sun from the acceleration site (which could be the flare site or the CME-driven shock). At present there is no consensus on the source of the energetic electrons detected in situ. While the low energy electrons responsible for the type II bursts are certainly due to CME driven shocks, the same cannot be said about the

higher energy electrons. The present results suggest that the flare size may hold some clue to understand the electron events. The good correlation between flare size and electron flux for the P and O events also suggest that the CME interaction has something to do with the observed electron intensity. The simplest explanation is that the preceding CMES somehow enable higher intensity to be observed at 1 AU. It is not clear how the CME interaction and flare size work in unison to produce the observed high electron intensity.

## 8. Discussion and Summary

We studied the large SEP events of solar cycle 23 to understand the correlation between their intensity and the speed of the associated CMES. While the overall correlation is similar to what was found before [*Kahler, 2001; Gopalswamy et al., 2003a*], the correlation improves remarkably for events with preceding CMES. The result also extends to energetic electrons, although the correlation coefficient is poorer. Excellent correlation was found for the group of events in which the primary CME interacted with a streamer or another eruption very close to the solar surface inferred from non-coronagraphic observations. The energetic electron intensity associated with CMES preceded by other wide CMES was better correlated with the flare size than with the CME speed. A combined effect of the preceding CMES and the flare size seems to have resulted in high electron flux. On the other hand, the proton intensity is not well correlated with flare size except for the O events in which the primary CME interacted with a possible preceding CME close to the Sun.

In addition to the high particle intensity, there may be other implications for the presence of preceding CMES. Considering the non-NP events, we see that in the majority of the SEP events (37/57 or 65%), the primary CME propagate through the aftermath

of preceding CMES, and not through the normal solar wind. Since the preceding CME is a multithermal plasma (8000 K in the prominence core to  $\sim 2$  MK in the front), the concept of “charge-state” freezing based solely on coronal temperatures may have to be revised. The observed charge states of SEP ions can be modified due to post-acceleration stripping when the ions transit through high density regions for a sufficiently long time [Reames *et al.*, 1999; Barghouty and Mewaldt, 2000]. In the scenario presented here, the preceding CMES can act as the high density region. CMES near the Sun represent a density enhancement of several times the ambient medium. If we consider a density ( $n$ ) of  $\sim 10^8$  cm $^{-3}$  in the preceding CME, and if the shock transit time ( $\tau$ ) through the density as  $\sim 0.5$  hr (as inferred from radio observations - see Gopalswamy *et al.*, 2001b), we get  $n\tau$  as  $1.8 \times 10^{11}$  cm $^{-3}$ s, which is more than adequate for additional stripping [Kovaltsov *et al.*, 2001].

It must be pointed out that we considered only preceding wide CMES, but there may be other smaller preceding events. We relaxed the width requirement to account for CMES with width  $< 60^\circ$ . There were 14 additional preceding CMES with widths ranging from  $15^\circ$  to  $30^\circ$ , distributed among the three groups as follows: P (4 events), NP (5 events), and O (5 events). Some primary CMES in the P group already have multiple preceding CMES, so allowing for additional preceding CMES does not change the result. For the O events, the interactions (streamer and under  $2 R_s$ ) are spatially closer to the primary CME so the interaction with the narrow CME has to occur later. For this reason, we ignore the narrow CMES preceding the O events. Moving the 5 NP events with preceding narrow CMES to the P group and repeating the analysis did not change the correlations significantly. The correlation coefficients decreased slightly for the P events and increased slightly for the

NP events. The main result that SEP events with preceding CMEs had a higher intensity did not change. Use of wide CMEs is still the best way to study the influence of preceding CMEs because it may be difficult to detect narrow CMEs originating from close to the disk center using coronagraphs.

The requirement that the preceding CME originates from the same active region as that of the primary CME was imposed to make sure that the CMEs interact. Therefore, we did not consider interaction of primary CMEs with CMEs from other solar sources. Since CMEs are large-scale structures, the coronal volume affected by fast and wide CMEs is generally very large especially at larger heliocentric distances. Therefore, even nearby eruptions can significantly affect particle acceleration and provide seed particles. Shock from one CME can propagate through a CME from a nearby region and may have similar effects [*Gopalswamy et al.*, 2003a].

The main conclusions of this paper are: (1) CMEs preceded by other wide CMEs within a day are more likely to be associated with high-intensity ( $> 50$  pfu) SEP events. (2) When the primary CMEs are not preceded by other wide CMEs, the resulting SEP event is of low intensity ( $< 50$  pfu) and the associated flares are generally weaker. (3) The proton intensity of SEP events with no preceding CMEs had no correlation with flare size; for events with preceding CMEs the correlation was extremely weak, but positive. (4) The flare size seems to play a major role in ordering the energetic electron intensity in those events where CME interaction is important. (5) The electron intensity is generally poorly correlated with the CME speeds, irrespective of the presence of a preceding CME. (6) For SEP events in which the primary CME interacted with a streamer or with an eruption preceding very close in time, both electron and proton intensities were highly

correlated with CME speed as well as flare size. This is somewhat puzzling and needs further investigation. (9) The scatter between CME speed and SEP intensity is reduced when the SEP events with and without preceding CMEs are considered separately.

**Acknowledgments.** We thank E. Aguilar-Rodriguez was checking the references. Part of this effort was also supported by the Air Force Office of Scientific Research (AFOSR), NASA/LWS and NSF/SHINE (ATM 0204588) programs. SOHO is a project of international cooperation between ESA and NASA.

## References

- Barghouty, A. F. and R. A. Mewaldt, Acceleration and Transport of Energetic Particles Observed in the Heliosphere, *AIP Conf. Proc.*, 528, p. 71, 2000.
- Brueckner, G. E. et al., The Large Angle Spectroscopic Coronagraph (LASCO), *Sol. Phys.*, 162, 357-402, 1995.
- Ciaravella, A., J. C. Raymond, A. van Ballegoijen, L. Strachan, A. Vourlidas, J. Li, J. Chen, & A. Panasyuk, *Astrophys. J.*, , 597, 1118, 2003
- Delaboudiniere, J.-P. et al., EIT: Extreme-Ultraviolet Imaging Telescope for the SOHO Mission, *Sol. Phys.*, 162, 291-312, 1995.
- Gopalswamy, N., Coronal Mass Ejections and Their Geospace Consequences, in *Probing the Sun with high resolution*, edited by S. C. Tripathy, and P. Venkatakrishnan, pp. 129, Narosa Publishing House, New Delhi, 2002.
- Gopalswamy, N., Solar and geospace connections of energetic particle events, *Geophys. Res. Lett.*, 30, SEP 1-1, 2003

- bibitem[Gopal2004a Gopalswamy, N., Interplanetary radio bursts, in Solar and Space Weather Radio Physics, ed. D. Gary and C. Keller, Kluwer, in press, 2004a.
- Gopalswamy, N., A global picture of CMEs in the inner heliosphere, in The Sun the Heliosphere as an integrated system, ed. G. Poletto and S. Suess, Kluwer, in press, 2004b.
- Gopalswamy, N., A. Lara, R. P. Lepping, M. L. Kaiser, D. Berdichevsky, & O. C. St. Cyr, Interplanetary acceleration of coronal mass ejections, *Geophys. Res. Lett.* Vol. 27 , No. 2 , p. 145, 2000a.
- Gopalswamy, N., M. L. Kaiser, B. J. Thompson, L. F. Burlaga, A. Szabo, A. Vourlidas, A. Lara, S. Yashiro, and J.-L. Bougeret, Radio-rich solar eruptive events, *Geophys. Res. Lett.*, 27, 1427, 2000b.
- Gopalswamy, N., A. Lara, M. L. Kaiser, and J.-L. Bougeret, Near-Sun and near-Earth manifestations of solar eruptions, *J. Geophys. Res.*, 106, 25261-25278, 2001a
- Gopalswamy, N., S. Yashiro, M. L. Kaiser, R. A. Howard, and J.-L. Bougeret, Radio signatures of coronal mass ejection interaction: Coronal mass ejection cannibalism?, *Astrophys. J.*, 548, L91, 2001b.
- Gopalswamy, N., S. Yashiro, M. L. Kaiser, R. A. Howard, and J.-L. Bougeret, Characteristics of coronal mass ejections associated with long wavelength type II radio bursts, *J. Geophys. Res.*, 106, 29219-29230, 2001c.
- Gopalswamy, N., S. Yashiro, G. Michalek, M. L. Kaiser, R. A. Howard, D. V. Reames, R. Leske, and T. von Roseninge, Interacting Coronal Mass Ejections and Solar Energetic Particles, *Astrophys. J.*, 572, L103-L107, 2002a.

- Gopalswamy, N., S. Yashiro, M. L. Kaiser, R. A. Howard, and J.-L. Bougeret, Interplanetary radio emission due to interaction between two coronal mass ejections, *Geophys. Res. Lett.*, *29*, 106, 2002b.
- Gopalswamy, N., Yashiro, S., Lara, A., Kaiser, M. L., Thompson, B. J., Gallagher, P. T., Howard, R. A., Large solar energetic particle events of cycle 23: A global view., *Geophys. Res. Lett.*, *30*, SEP 3-1, 2003a.
- Gopalswamy, N., A. Lara, S. Yashiro, S. Nunes, S. & R. A. Howard, ESA SP-535: Solar Variability as an Input to the Earth's Environment, 403, 2003b
- Kahler, S. W., Injection profiles of solar energetic particles as functions of coronal mass ejection heights, *Astrophys. J.*, *428*, 837-842, 1994.
- Kahler, S. W., The correlation between solar energetic particle peak intensities and speeds of coronal mass ejections: Effects of ambient particle intensities and energy spectra, *J. Geophys. Res.*, *106*, 20947-20955, 2001.
- Kahler, S. W., E. Hildner, and M. A. I. van Hollebeke, Prompt solar proton events and coronal mass ejections, *Sol. Phys.*, *57*, 429-443, 1978
- Kallenrode, M.-B, Magnetic clouds and interplanetary particle transport: a numerical model *Journal of Atmospheric and Terrestrial Physics*, *64*, 1973, 2002.
- Kovaltsov, G. A., A. F. Barghouty, L. Kocharov, V. M., Ostryakov, and J. Torsti, J., Charge-equilibration of Fe ions accelerated in a hot plasma, *Astron. Astrophys.*, *375*, 1075, 2001.
- Lin, R. P. et al., A Three-Dimensional Plasma and Energetic Particle Investigation for the Wind Spacecraft, *Space Sci. Rev.*, *71*, 125-153, 1995.

- Mason, G. M., J. E. Mazur, & J. R. Dwyer,  $^3\text{He}$  Enhancements in Large Solar Energetic Particle Events, *Astrophys. J.*, , 525, L133, 1999.
- Nakajima, H., et al., The Nobeyama Radioheliograph, *Proc. IEEE*, 82, 705, 1994
- Obayashi, T., Propagation of Solar Corpuscles and Interplanetary Magnetic Fields, *J. Geophys. Res.*, , 67, 1717, 1962.
- Reames, D. V., Particle acceleration at the Sun and in the heliosphere, *Space Sci. Rev.*, 90, 413, 1999.
- Reames, D. V., C. K. Ng, and A. J. Tylka, Energy-dependent ionization states of shock-accelerated particles in the solar corona, *Geophys. Res. Lett.*, 26, 3585, 1999.
- Stewart, R. T., Moving Type IV bursts, in Solar radiophysics, *Studies of emission from the sun at metre wavelengths*, Cambridge and New York, p. 361, 1985.
- Stewart, R. T., M. K. McCabe, M. J. Koomen, R. T. Hansen, and G. A. Dulk, Observations of Coronal Disturbances from 1 to 9 R<sub>sun</sub>. I: First Event of 1973, January 11, *Sol. Phys.*, 36, 203, 1974.
- Vourlidis, A., D. Buzasi, R. A. Howard, and E. Esfandiari, Solar variability: from core to outer frontiers, Ed. A. Wilson. ESA SP-506, Vol. 1. Noordwijk: ESA Publications Division, p. 91, 2002.
- Yashiro, S., N. Gopalswamy, G. Michałek, O. C. St.Cyr, S. P. Plunkett, N. B. Rich, and R. A. Howard, A catalog of white light coronal mass ejections observed by the SOHO spacecraft, accepted by JGR.



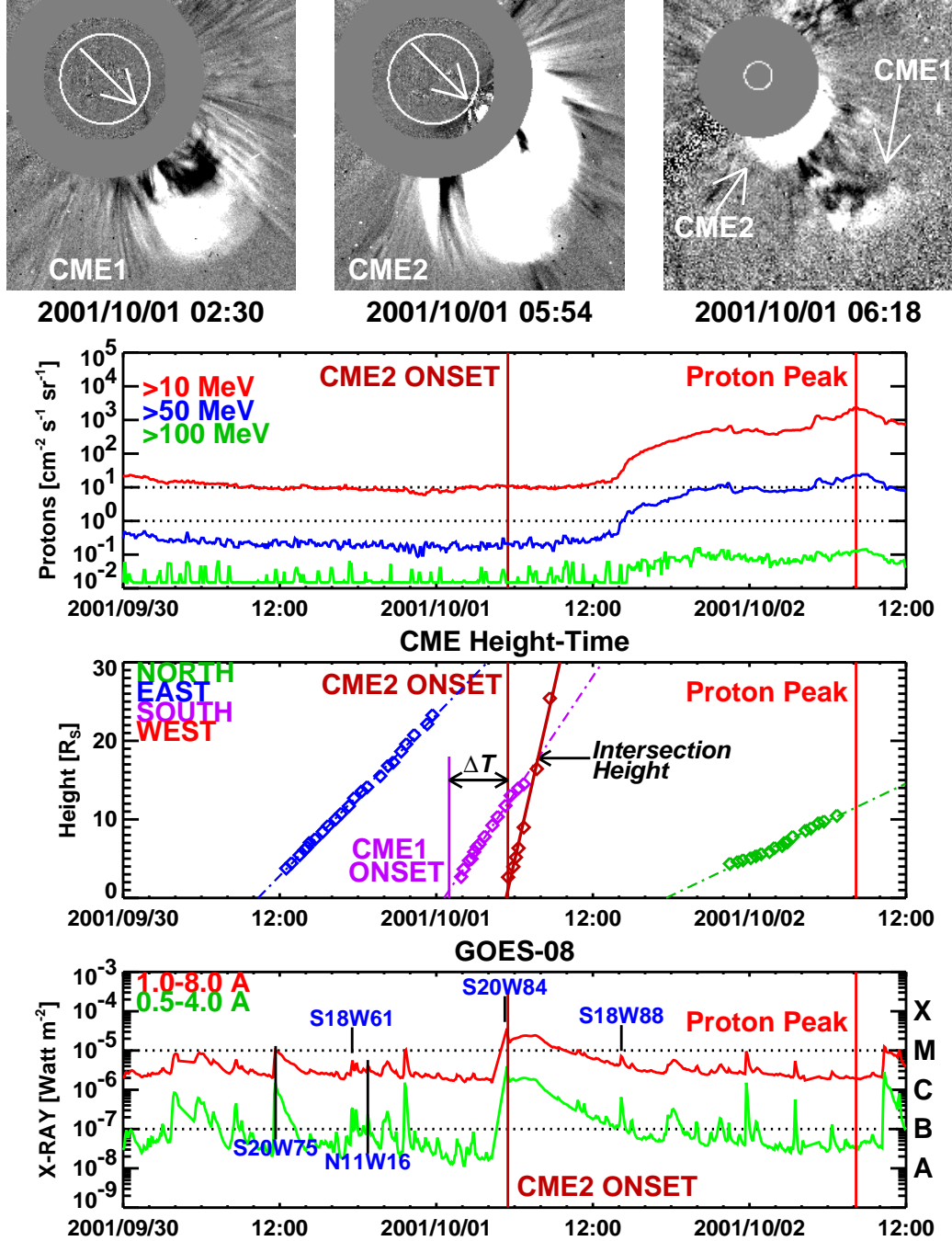


**Figure 1.** An example of P events that occurred on 2001 October 1 (event #36 in Table 1). (top) LASC0 difference images showing the preceding (CME1) and primary (CME2) CMES. The 06:18 UT images shows both the CMES in a single frame. (upper middle) SEP intensity profiles in three energy channels (>10 MeV, > 30 MeV, and > 100 MeV). The onset time of the primary CME and the time of peak intensity of the protons are marked. (lower middle) CME activity around the time of the primary CME shown as height-time plots. The plots are color coded to show the direction of the central position angle. The onset time of the preceding CME (CME1) is also marked. The onset time difference ( $\Delta T$ ) between the primary and preceding CMES is also indicated. The height at which the primary and preceding CMES intersect is also noted. (bottom) GOES X-ray light curves showing the flare activity associated with the two CMES. The heliographic location of the flares are also indicated. The active region from which the CMES were launched was located at S20W84 at the time of the primary CME.

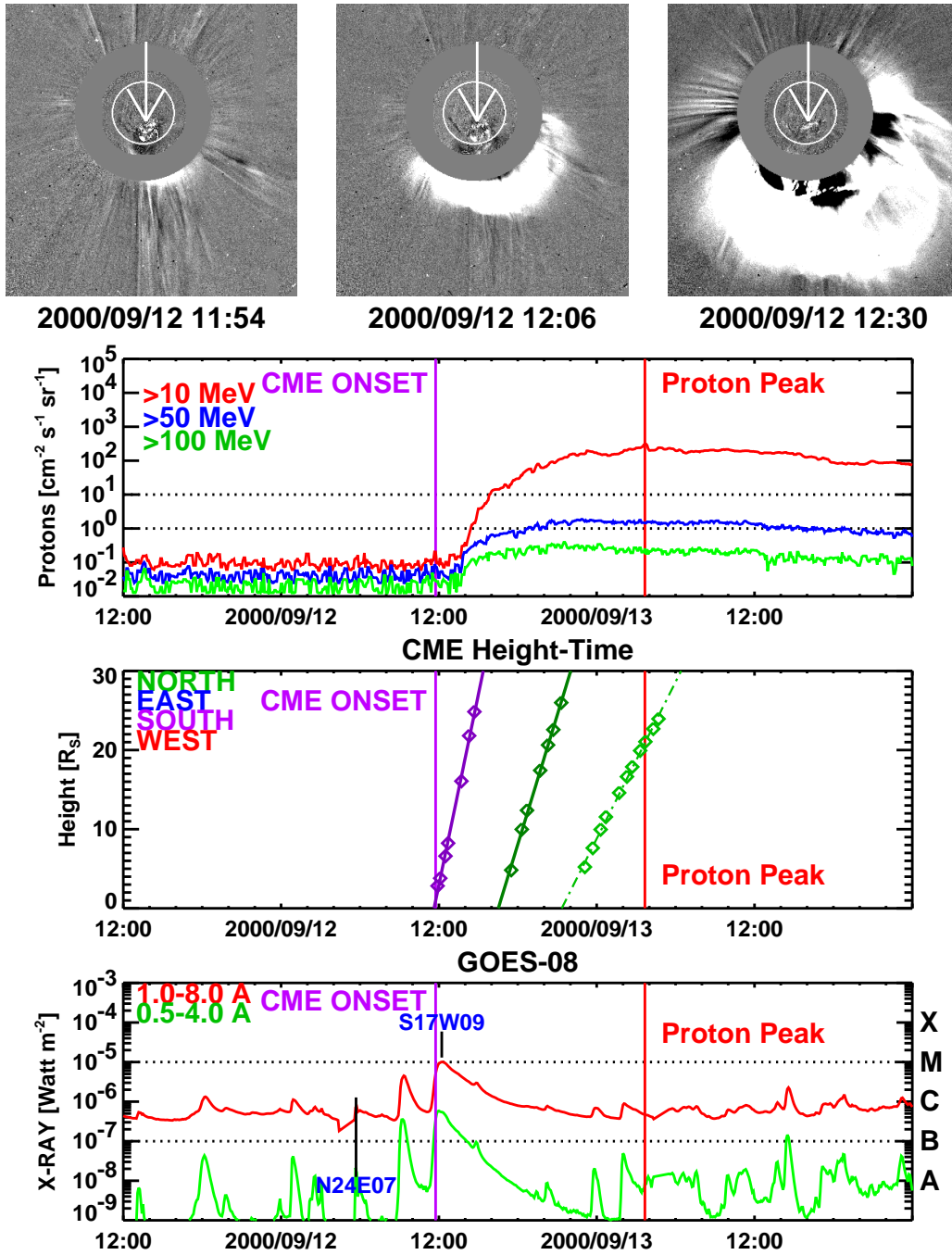
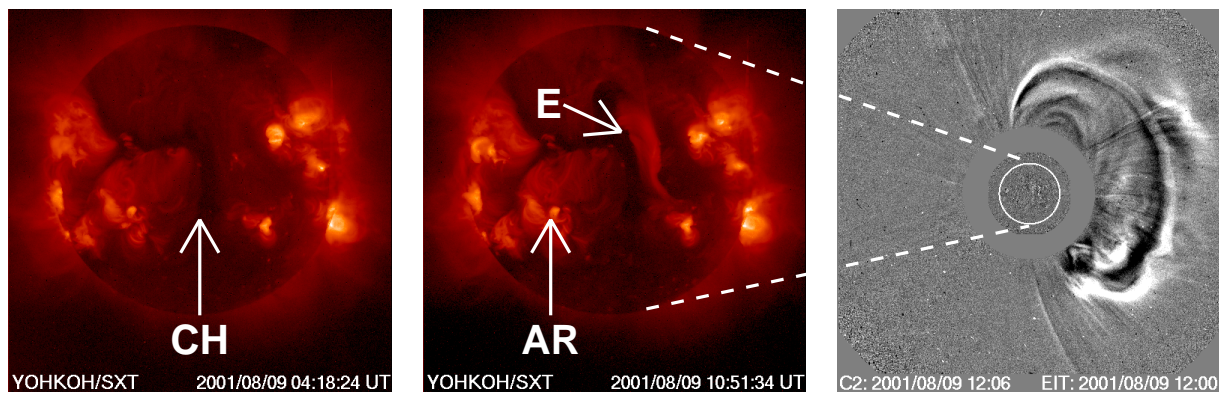
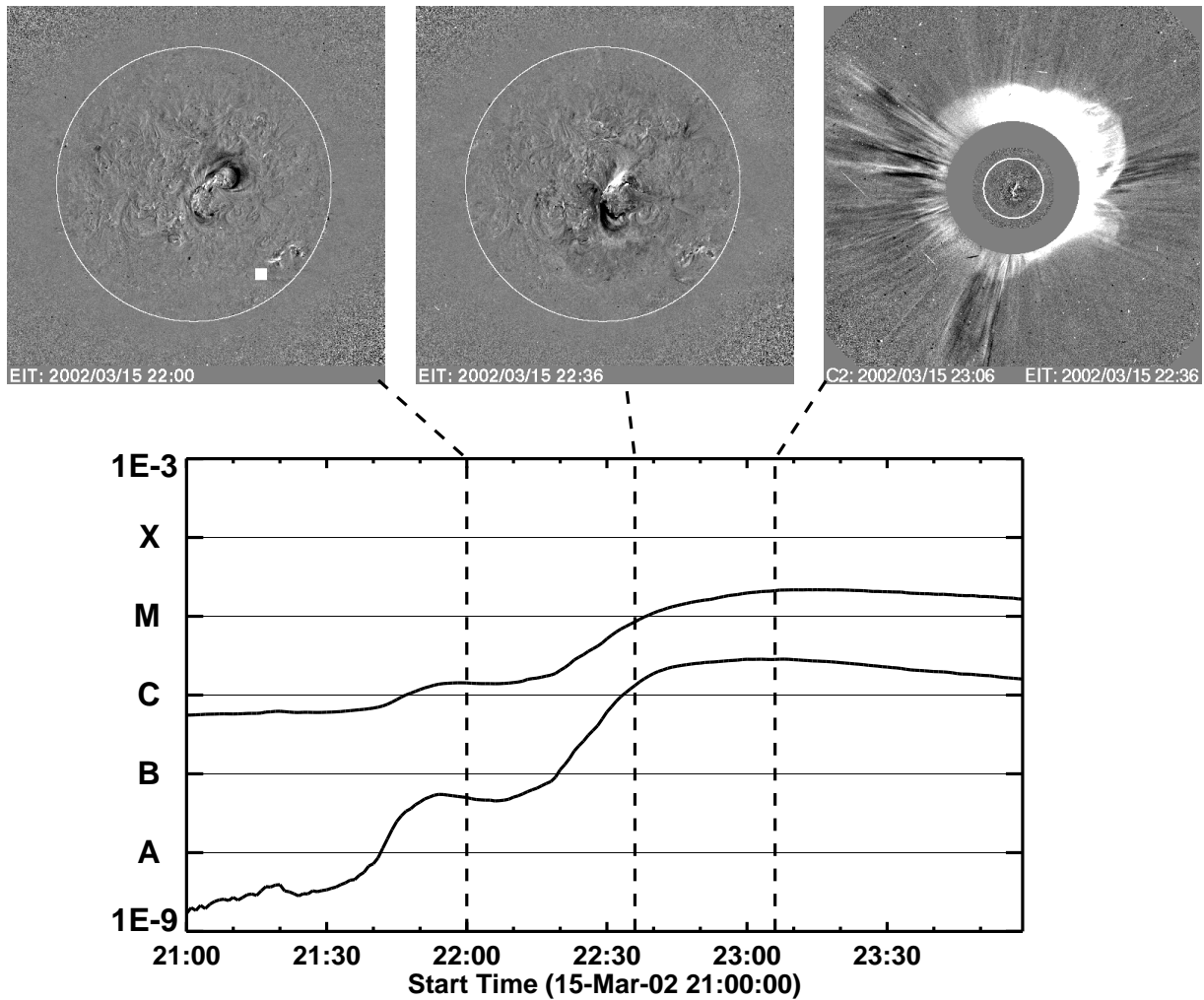


Figure 2. An example of the NP events (event #17 in Table 1). The plots are similar to those of Fig. 1, except that there is no preceding CME. The primary CME occurred on 2000 September 12.



**Figure 3.** Two Yohkoh/SXT images on 2001 August 09 at 04:18 and 10:51 UT, showing the coronal hole (CH) and the SXT arcade (E). The LASCO difference image at 12:06 UT shows a white light CME associated with the SXT arcade. This CME seems to be too early to be associated with the SEP event of 2001 August 09. Even though the solar source was close to the disk center, the CME moved mostly to the west probably because of the extended coronal hole immediately to the east of the CME source region. Also marked is active region 9570 (AR), from which an EUV eruption was observed later in the day at 18:22 UT by EIT (but not by LASCO).



**Figure 4.** An example (2002 March 15, event #48 in Table 1) of SEP events in which the primary CME is likely to have interacted with a possible preceding CME below the occulting disk of LASCOCO/C2. Images from SOHO/EIT and LASCOCO/C2 are shown at the top. The times of the images are marked on the GOES X-ray plot. The GOES plot as well as the EIT images clearly show two eruptions from the same region, but LASCOCO sees only a single CME. The LASCOCO CME is likely to be a compound CME if both EIT eruptions had associated mass ejections.

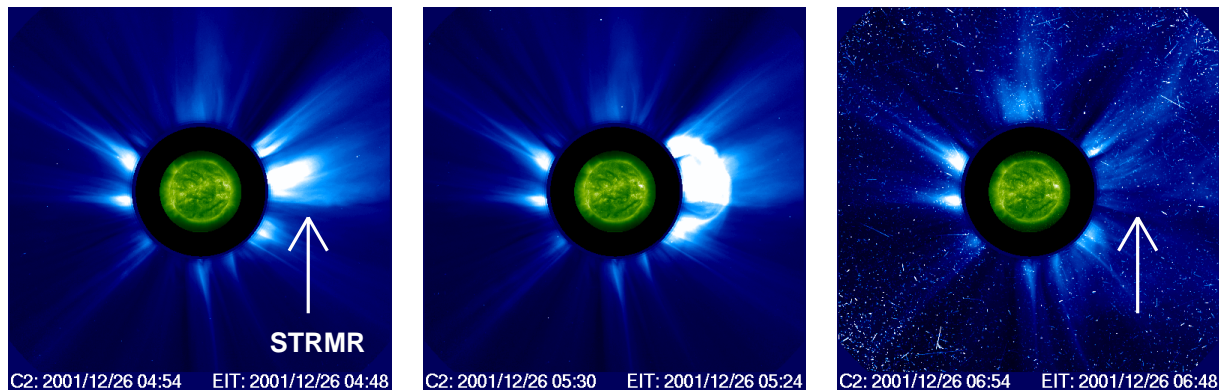


**Figure 5.** An example (2001 December 26 CME, event #43 in Table 1) of the streamer interaction events. The preexisting streamer is marked ‘STRMR’ in the 04:54 UT LASCO image. The CME can be seen in the 05:30 LASCO image with the superposed EIT image showing the solar source as a compact brightening near the west limb. The LASCO image at 06:54 shows that the streamer is gone with the CME.

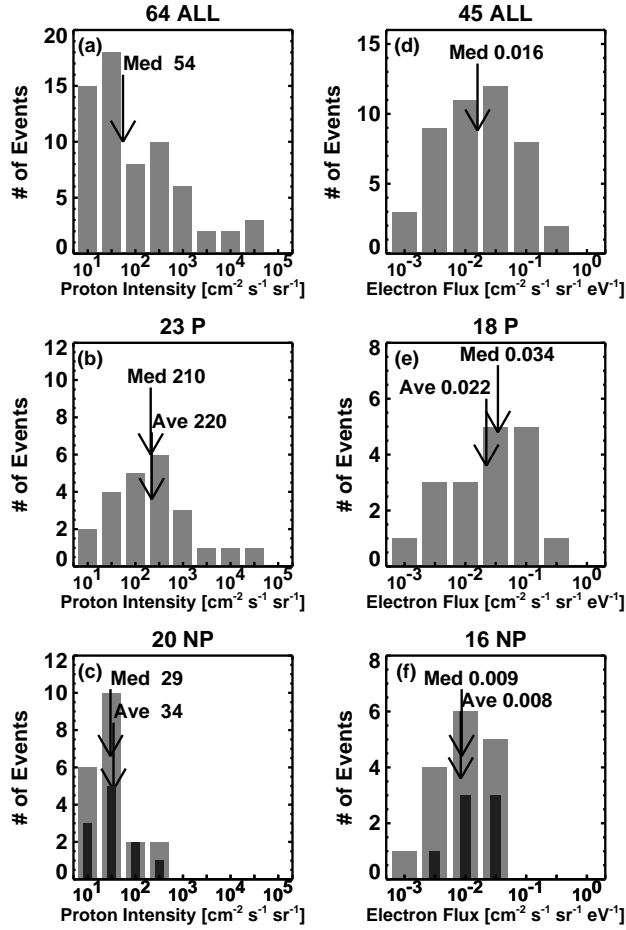


**Figure 6.** The distribution of intensities for proton events (a-c) and electron events (d-f). For both protons and electrons, the intensity of P events (b,e) extends to much larger values than for the NP events (c,f). The mean (‘Ave’) and median (‘Med’) values of the distributions are marked. The darker histograms in (c) and (f) correspond to front-sided events. The mean and median values for the front-sided proton events in (c) are 38 and 34 pfu, respectively; the corresponding values are 0.014 and 0.013 efu for the electron events in (f).

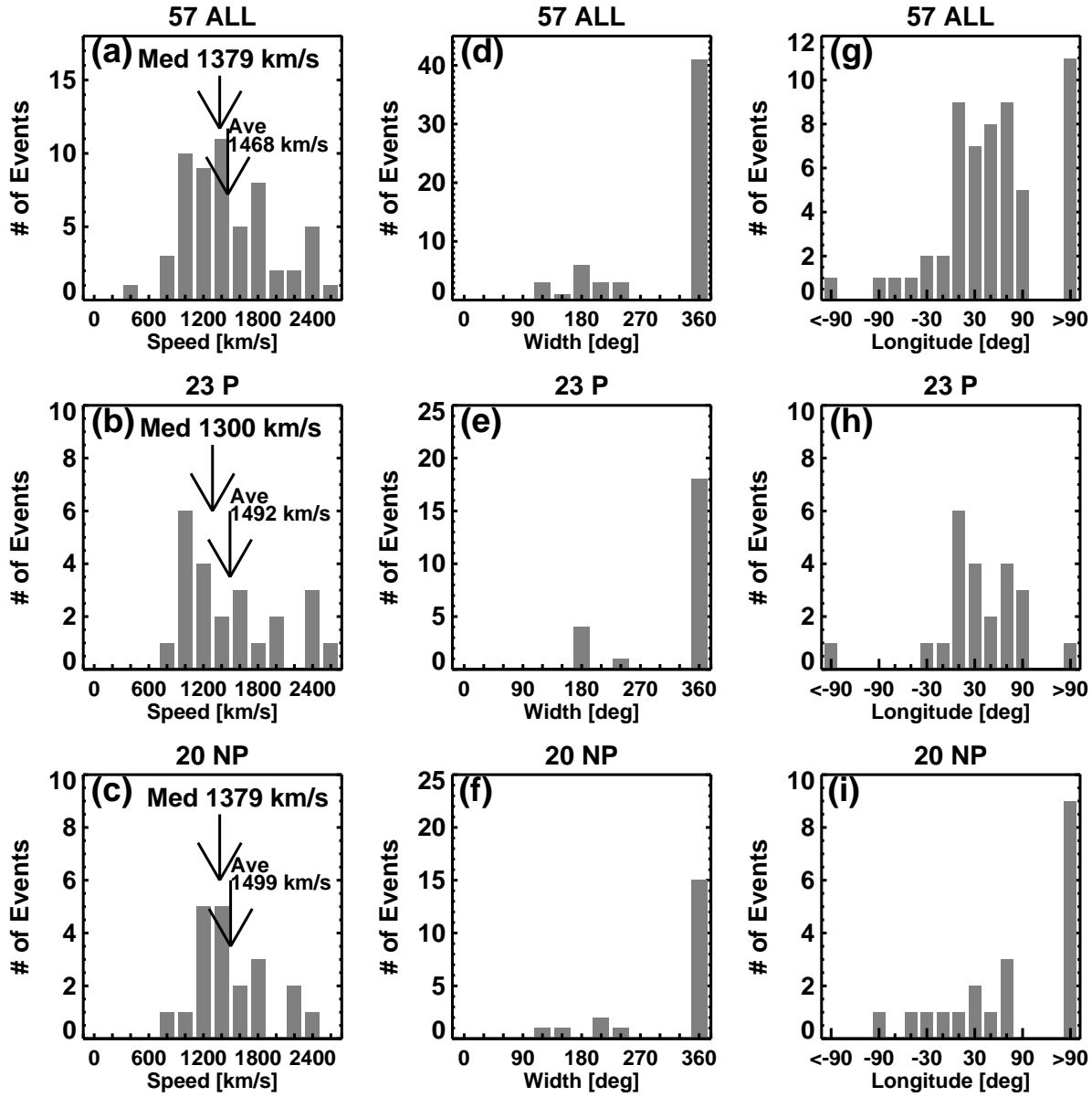


**Figure 7.** The speed, width and source longitude distributions of the primary CMEs associated with the P and NP events in comparison with those of all the 57 SEP events. The three groups have very similar speeds and widths. The fraction of behind-the-limb CMEs is larger for the NP events.

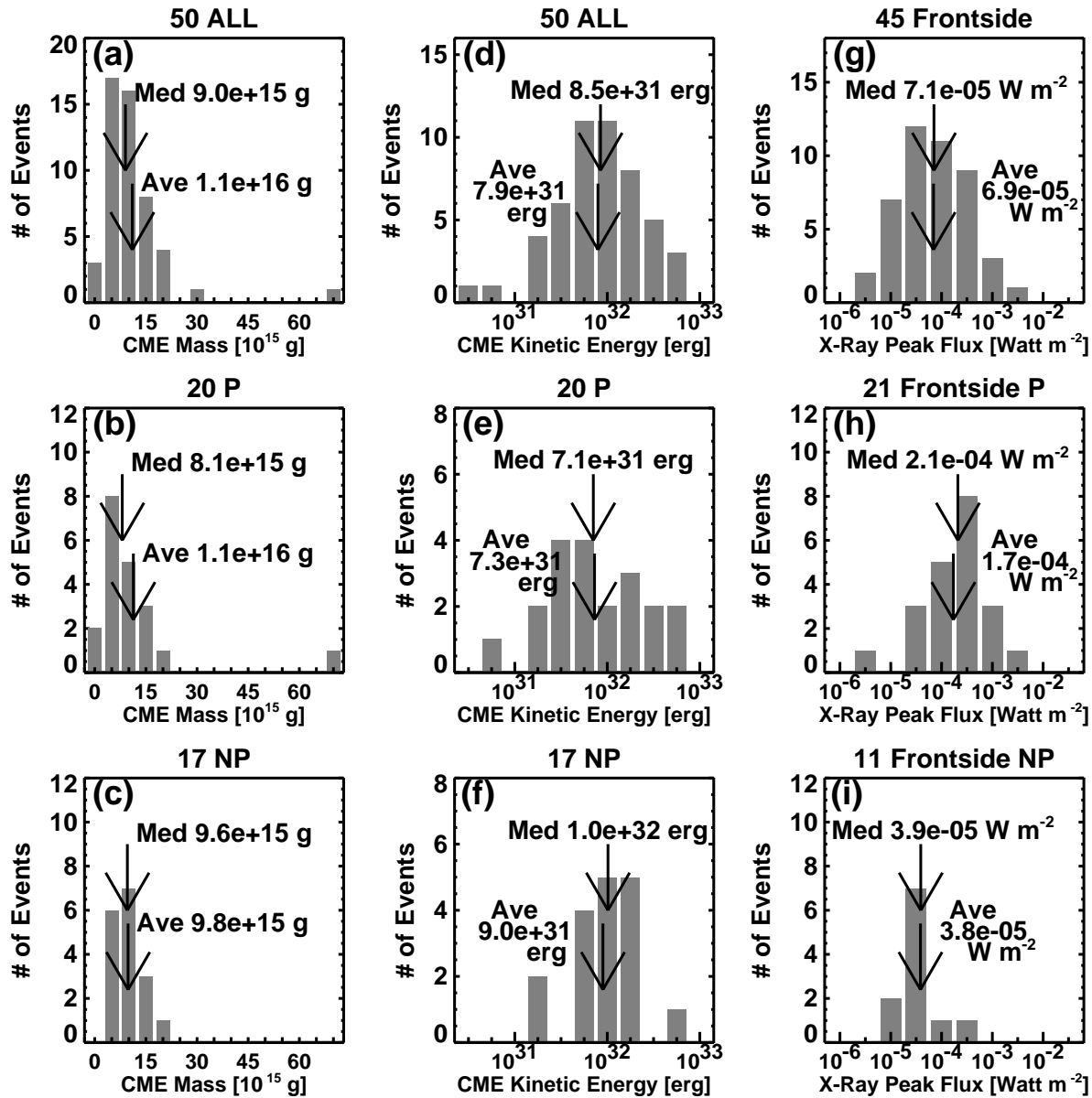


**Figure 8.** The distributions of CME mass, kinetic energy and the size of the associated soft X-ray flare for the P and NP events in comparison with those of all the 57 events. The mean and median values of the distributions are indicated. The GOES soft X-ray flux (in units of  $Wm^{-2}$ ) in the 1-8 Å channel is used as a measure of the flare size.

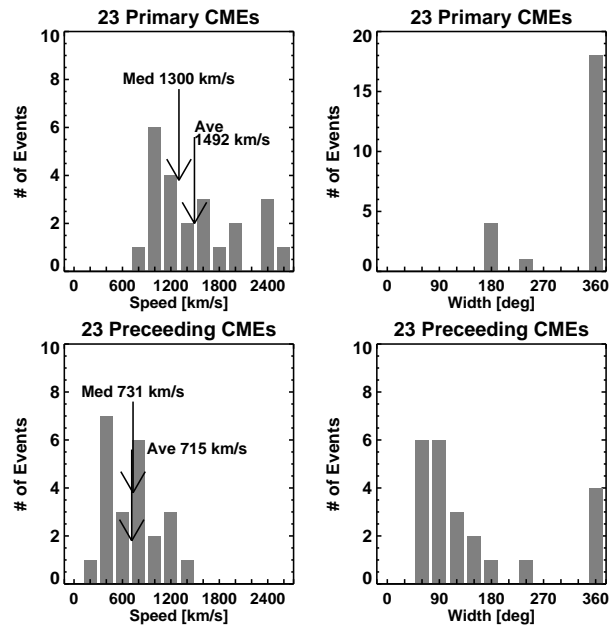


**Figure 9.** The speed and width distributions of the preceding CMEs as compared to those of primary CMEs. The mean and median values of the distributions are indicated.

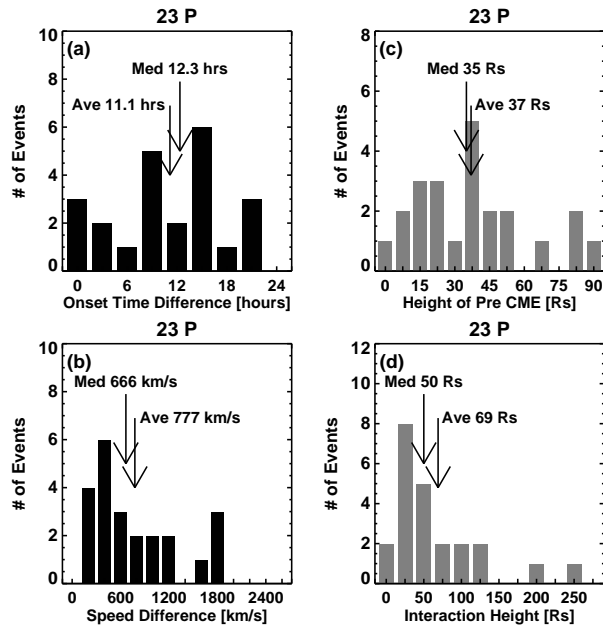


**Figure 10.** The distribution of (a) temporal separation ( $\Delta T$ ), (b) approaching speed ( $\Delta V$ ), (c) initial spatial separation ( $\Delta R$ ) between the primary and preceding CMES (Table 2), and (d) the height at which the trajectories of the primary and preceding CMES intersect. The mean and median values of the distributions are indicated.

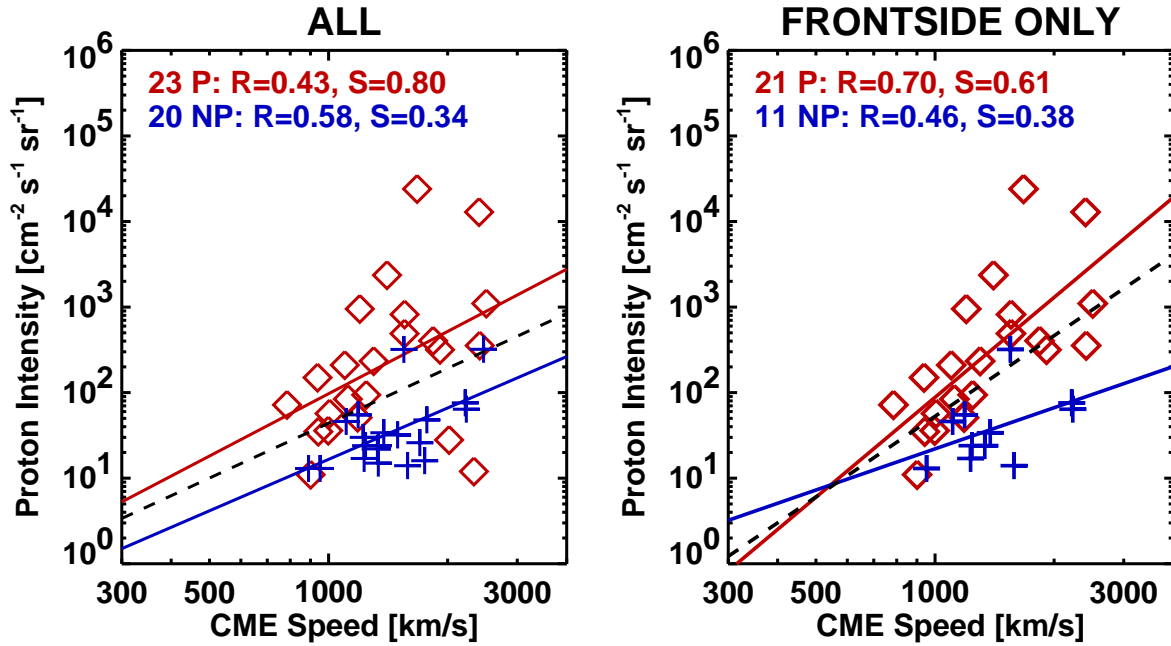


**Figure 11.** (left)  $I_p - V_{cme}$  scatter plot for the P (diamond symbols) and NP (plus symbols) events. (right) the same as in the left but for frontside events (central median distance  $\leq 90^\circ$ ). The solid lines are the regression lines to the P and NO data points. The dashed line is the regression line for all the data points. Here and in the following figures, S denotes the standard deviation of the Y-variable. R is the correlation coefficient. Note that the P and NP data points occupy different regions of the plot with minimal overlap.

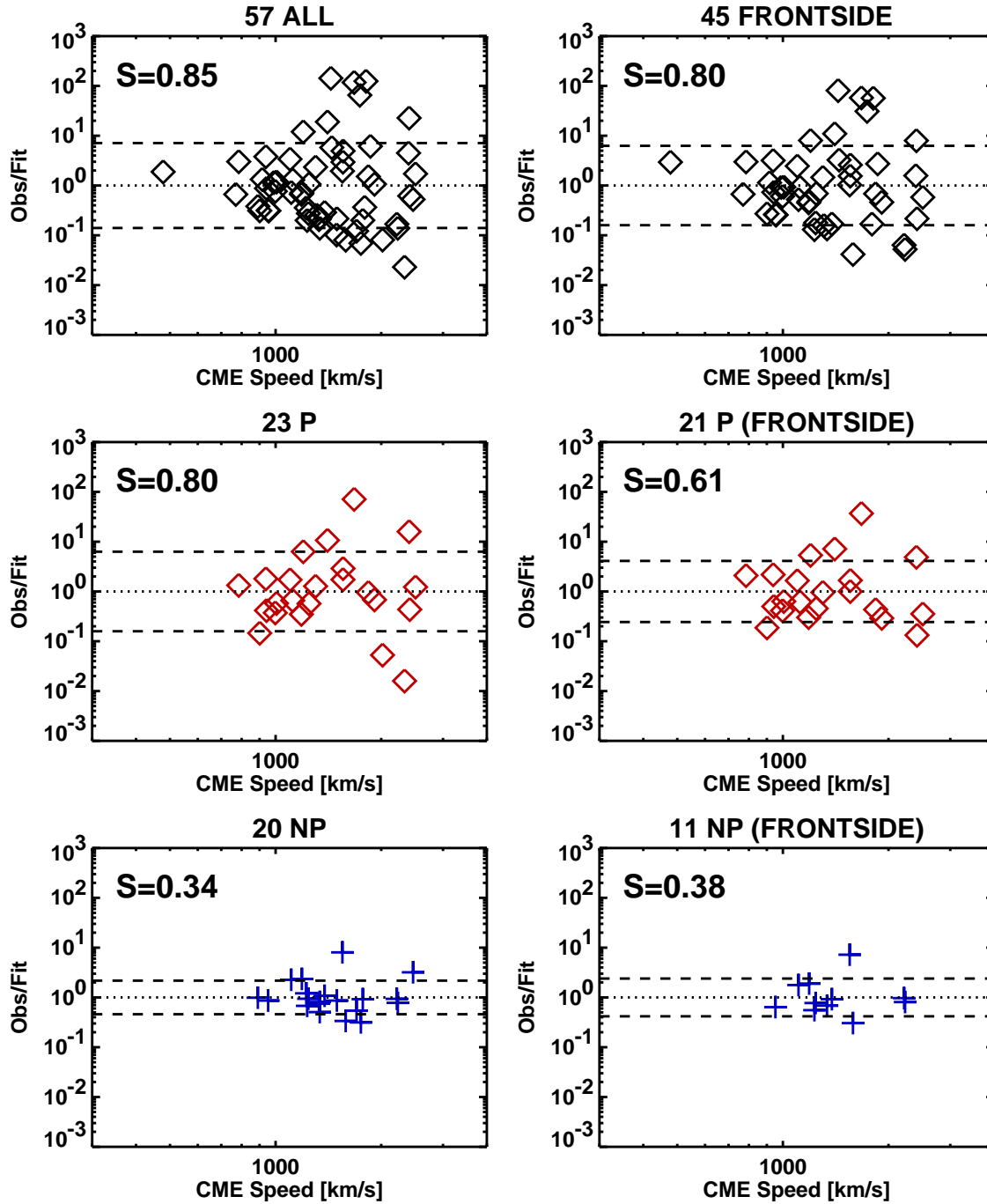


**Figure 12.** Extents of scatter between proton intensity and CME speed for the P (middle panels) and NP (lower panels) in comparison with that for all the 57 events (top panels), plotted as the ratio of the observed (Obs) intensity to the intensity given by the regression line (Fit). Plots are made for all events (left panels) and front-sided events (right panels). As before, the right panels corresponds to frontside events.

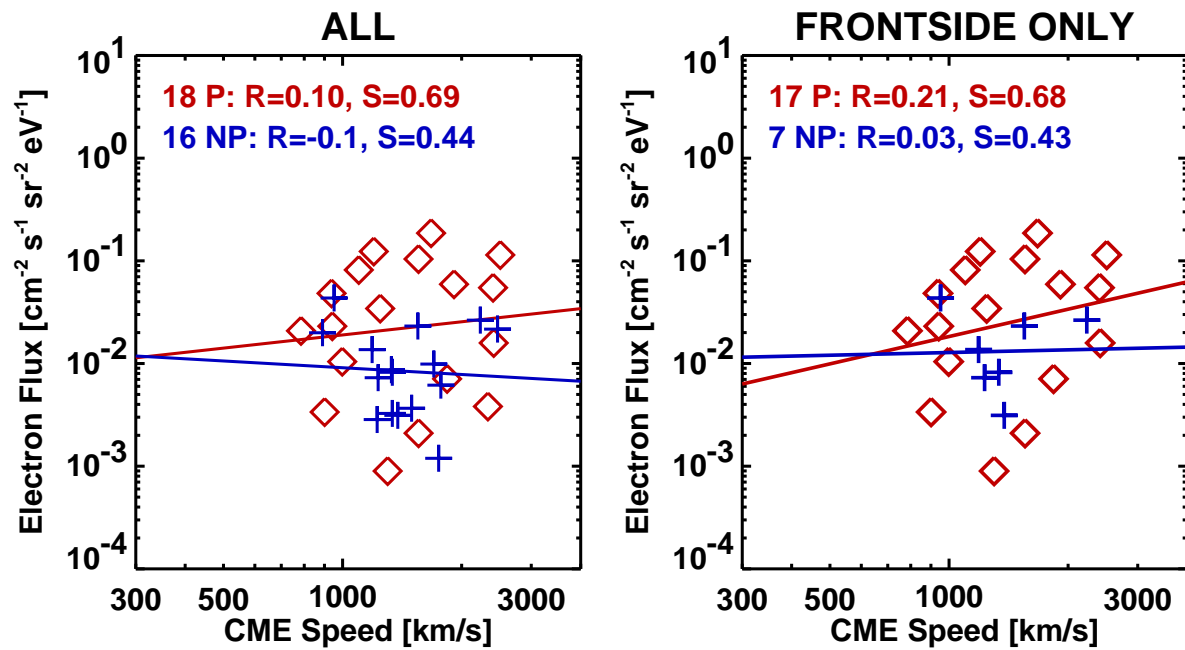


**Figure 13.** The scatter plots between the 108 keV electron intensity and CME speed for the P (diamond symbols) and NP (plus symbols) events. The solid lines are the best-fit lines for the data points in each group.

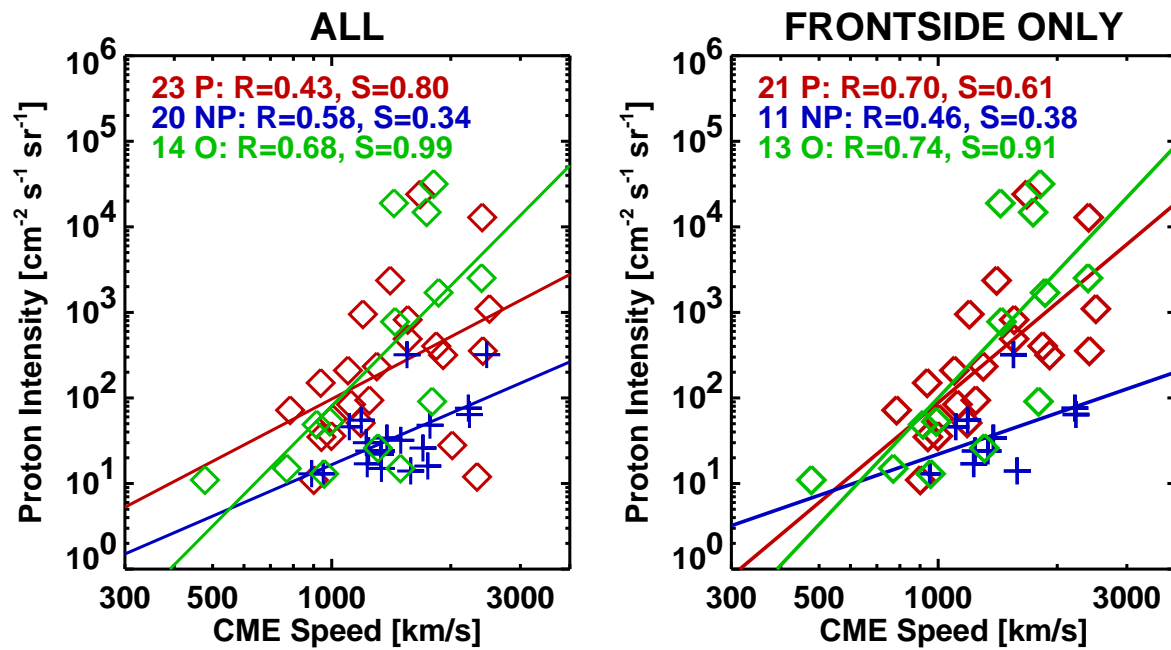


**Figure 14.** The scatter plots between proton intensity and CME speed for the P, NP, and O groups. The regression line is also shown for each group. The correlation coefficients are also indicated.

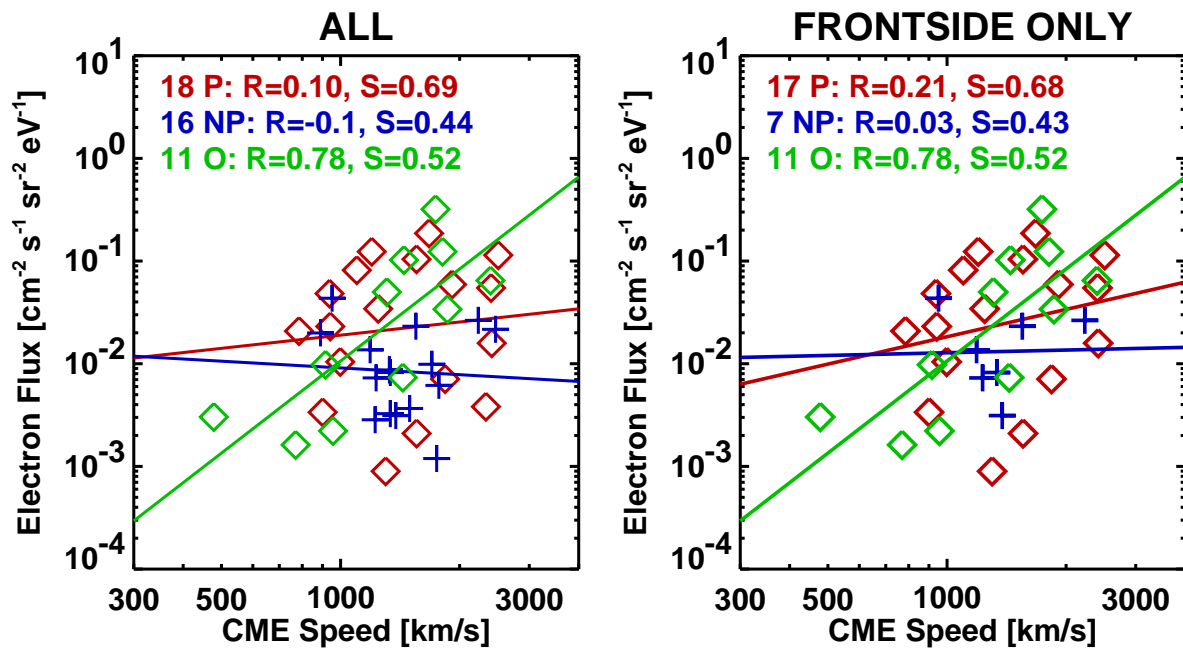
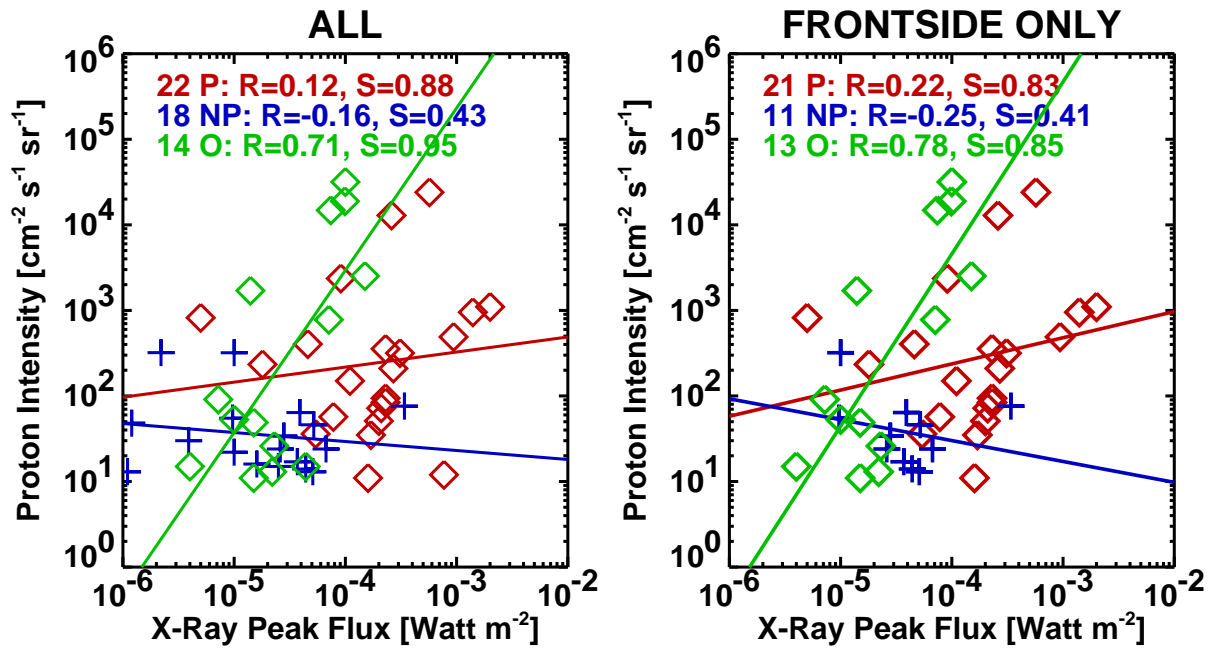


Figure 15. The scatter plots between the 108 keV electron intensity and CME speed for the P, NP, and O groups. The regression line is also shown for each group. The correlation coefficients are also indicated.



**Figure 16.** The scatter plots between proton intensity and flare size for the P, NP and O groups. The regression line is also shown for each group. The correlation coefficients are also indicated.

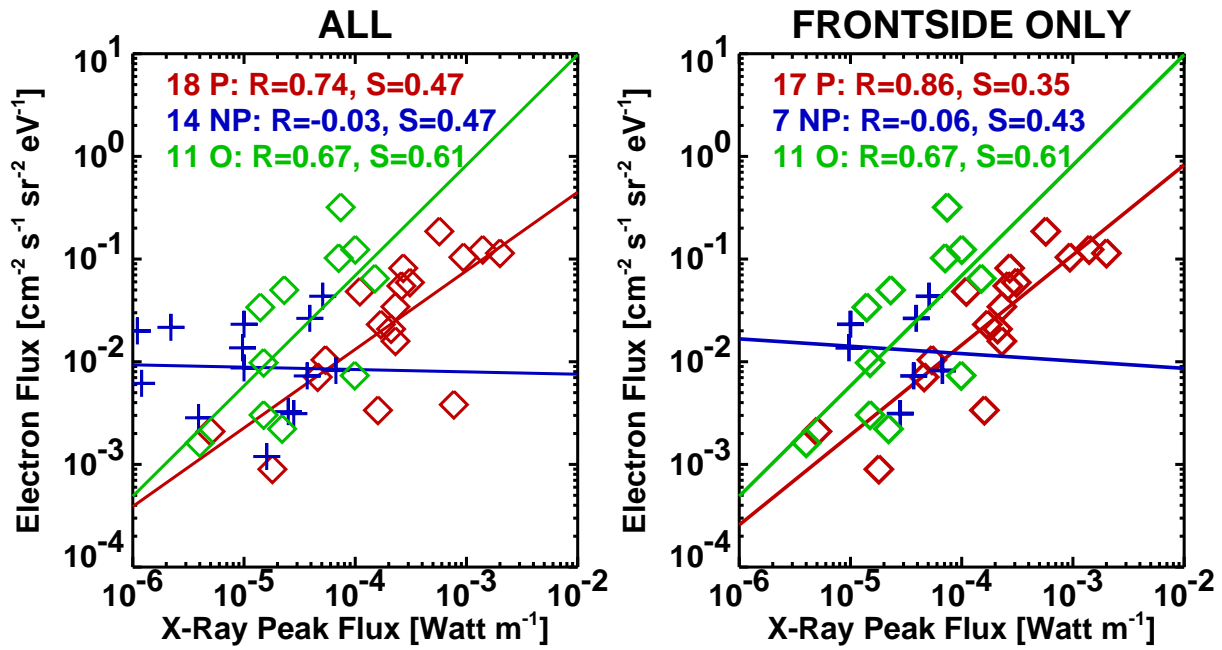


Figure 17. Scatter plots between the 108 keV electron intensity and flare size for the P, NP and O groups. The regression line is also shown for each group. The correlation coefficients are also indicated.